Self-organization approach for THz polaritonic metamaterials

A. Reyes-Coronado,[1,2,*] M. F. Acosta,[3] R. I. Merino,[3] V. M. Orera,[3] G. Kenanakis,[1,4] N. Katsarakis,[1,4] M. Kafesaki,[1,5] Ch. Mavidis,[1,5] J. García de Abajo,[6] E. N. Economou,[1] and C. M. Soukoulis[1,7]

[1]*Institute of Electronic Structure and Laser (IESL), Foundation for Research and Technology-Hellas (FORTH), P.O. Box 1385, 71110 Heraklion, Crete, Greece*
[2]*Instituto de Física, Benemérita Universidad Autónoma de Puebla, Apartado Postal J-48, Puebla, Pue. 72570, Mexico*
[3]*Instituto de Ciencia de Materiales de Aragón, CSIC-Universidad de Zaragoza, E-50009 Zaragoza, Spain*
[4]*Science Department, Technological Educational Institute of Crete, 71004 Heraklion, Crete, Greece*
[5]*Department of Material Science and Technology, University of Crete, 71003 Heraklion, Crete, Greece*
[6]*Instituto de Química Física, Rocasolano, Serrano 119, 28006 Madrid, Spain*
[7]*Ames Laboratory-USDOE, and Department of Physics and Astronomy, Iowa State University, Ames, Iowa 50011, USA*
**a.reyescoronado@gmail.com*

Abstract: In this paper we discuss the fabrication and the electromagnetic (EM) characterization of anisotropic eutectic metamaterials, consisting of cylindrical polaritonic LiF rods embedded in either KCl or NaCl polaritonic host. The fabrication was performed using the eutectics directional solidification self-organization approach. For the EM characterization the specular reflectance at far infrared, between 3 THz and 11 THz, was measured and also calculated by numerically solving Maxwell equations, obtaining good agreement between experimental and calculated spectra. Applying an effective medium approach to describe the response of our samples, we predicted a range of frequencies in which most of our systems behave as homogeneous anisotropic media with a hyperbolic dispersion relation, opening thus possibilities for using them in negative refractive index and imaging applications at THz range.

© 2012 Optical Society of America

OCIS codes: (160.3918) Metamaterials; (160.1190) Anisotropic optical materials; (220.4000) Microstructure fabrication; (160.1245) Artificially engineered materials; (160.4760) Optical properties; (160.4670) Optical materials.

References and links

1. R. Köhler, A. Tredicucci, F. Beltram, H. E. Beere, E. H. Linfield, A. G. Davies, D. A. Ritchie, R. C. Iotti, and F. Rossi, "Terahertz semiconductor-heterostructure laser," Nature **417**, 156–159 (2002).
2. S. W. Smye, J. M. Chamberlain, A. J. Fitzgerald, and E. Berry, "The interaction between Terahertz radiation and biological tissue," Phys. Med. Biol. **46**, R101–R112 (2001).
3. D. L. Woolard, J. O. Jensen, R. J. Hwu, and M. S. Shur, *Terahertz Science and Technology for Military and Security Applications* (World Scientific Publishing Co. Pte. Ltd., 2007).
4. T. Edwards, *Gigahertz and Terahertz Technologies for Broadband Communications* (Artech House Inc., 2000).

#161382 - $15.00 USD Received 12 Jan 2012; revised 19 Apr 2012; accepted 23 Apr 2012; published 15 Jun 2012

5. V. Minier, G. Durand, P.-O. Lagage, M. Talvard, T. Travouillon, M. Busso, and G. Tosti, "Submillimetre/terahertz astronomy at dome C with CEA filled bolometer array," EAS Publications Series **25**, 321–326 (2007).
6. V. G. Veselago, "The electrodynamics of substances with simultaneously negative values of ε and μ," Sov. Phys. Usp. **10**, 509–514 (1968).
7. J. B. Pendry, "Negative refraction makes perfect lens," Phys. Rev. Lett. **85**, 3966–3969 (2000).
8. J. B. Pendry, A. J. Holden, D. J. Robbins, and W. J. Stewart, "Magnetism from conductors and enhanced nonlinear phenomena," IEEE Trans. Microw. **47**, 2075–2084 (1999).
9. J. B. Pendry, A. J. Holden, D. J. Robbins, and W. J. Stewart, "Low frequency plasmons in thin-wire structures," J. Phys.: Condens. Matter **10**, 4785–4809 (1998).
10. D. R. Smith, W. J. Padilla, D. C. Vier, S. C. Nemat-Nasser, and S. Schultz, "Composite medium with simultaneously negative permeability and permittivity," Phys. Rev. Lett. **84**, 4184–4187 (2000).
11. S. O'Brien and J. B. Pendry, "Photonic band-gap effects and magnetic activity in dielectric composites," J. Phys.: Condens. Matter **14**, 4035–4044 (2002).
12. J. A. Schuller, R. Zia, T. Taubner, and M. L. Brongersma, "Dielectric metamaterials based on electric and magnetic resonances of silicon carbide particles," Phys. Rev. Lett. **99**, 107401 (2007).
13. L. Jylhä, I. Kolmakov, S. Maslovski, and S. Tretyakov, "Modeling of isotropic backward-wave materials composed of resonant spheres," J. Appl. Phys. **99**, 043102 (2006).
14. N. W. Ashcroft and N. D. Mermin, *Solid State Physics* (Sanders College Publishing/Harcourt Brace, 1976).
15. V. Yannopapas and A. Moroz, "Negative refractive index metamaterials from inherently non-magnetic materials for deep infrared to terahertz frequency ranges," J. Phys.: Condens. Matter **17**, 3717–3734 (2005).
16. D. R. Smith and D. Schurig, "Electromagnetic wave propagation in media with indefinite permittivity and permeability tensors," Phys. Rev. Lett. **90**, 077405 (2003).
17. M. A. Noginov, Yu. A. Barnakov, G. Zhu, T. Tumkur, H. Li, and E. E. Narimanov, "Bulk photonic metamaterial with hyperbolic dispersion," App. Phys. Lett. **94**, 151105 (2009).
18. M. A. Noginov, Y. A. Barnakov, G. Zhu, T. Tumkur, L. Heng, and E. E. Narimanov, "Bulk metamaterial with hyperbolic dispersion," Conference on lasers and electro-optics/International quantum electronics conference, OSA technical digest (CD) (Optical Society of America, 2009), paper JWC2.
19. T. Tumkur, G. Zhu, P. Black, Yu. A. Barnakov, C. E. Bonner, and M. A. Noginov, "Control of spontaneous emission in a volume of functionalized hyperbolic metamaterial," App. Phys. Lett. **99**, 151115 (2011).
20. A. Reyes-Coronado, M. F. Acosta, R. I. Merino, V. M. Orera, G. Kenanakis, N. Katsarakis, M. Kafesaki, and C. M. Soukoulis, "Electromagnetic response of anisotropic eutectic metamaterials in THz range," AIP Conf. Proc. **1291**, 148–150 (2010).
21. H. Lee, Z. Liu, Y. Xiong, C. Sun, and X. Zhang, "Development of optical hyperlens for imaging below the diffraction limit," Opt. Express **15**, 15886–15891 (2007).
22. Z. Liu, H. Lee, Y. Xiong, C. Sun, and X. Zhang, "Far-field optical hyperlens magnifying sub-diffraction-limited objects," Science **315**, 1686–1686 (2007).
23. Z. Jacob, L. V. Alekseyev, and E. Narimanov, "Optical hyperlens: far-field imaging beyond the diffraction limit," Opt. Express **14**, 8247–8256 (2006).
24. A. Salandrino and N. Engheta, "Far-field subdiffraction optical microscopy using metamaterial crystals: theory and simulations," Phys. Rev. B **74**, 075103 (2006).
25. A. Fang, T. Koschny, and C. M. Soukoulis, "Optical anisotropic metamaterials: negative refraction and focusing," Phys. Rev. B **79**, 245127 (2009).
26. G. A. Wurtz, W. Dickson, D. O'Connor, R. Atkinson, W. Hendren, P. Evans, R. Pollard, and A. V. Zayats, "Guided plasmonic modes in nanorod assemblies: strong electromagnetic coupling regime," Opt. Express **16**, 7460–7470 (2008).
27. N. Liu, H. Guo, L. Fu, S. Kaiser, H. Schweizer, and H. Giessen, "Three-dimensional photonic metamaterials at optical frequencies," Nat. Mater. **7**, 31–37 (2008).
28. J. Valentine, S. Zhang, T. Zentgraf, E. Ulin-Avila, D. A. Genov, G. Bartal, and X. Zhang, "Three-dimensional optical metamaterial with a negative refractive index," Nature **455**, 376–379 (2008).
29. J. K. Gansel, M. Thiel, M. S. Rill, M. Decker, K. Bade, V. Saile, G. von Freymann, S. Linden, and M. Wegener, "Gold helix photonic metamaterial as broadband circular polarizer," Science **325**, 1513–1515 (2009).
30. D. B. Burckel, J. R. Wendt, G. A. Ten Eyck, A. R. Ellis, I. Brener, and M. B. Sinclair, "Fabrication of 3D metamaterial resonators using self-aligned membrane projection lithography," Adv. Mater. **22**, 3171–3175 (2010).
31. C. Rockstuhl, F. Lederer, C. Etrich, T. Pertsch, and T. Scharf, "Design of an artificial three-dimensional composite metamaterial with magnetic resonances in the visible range of the electromagnetic spectrum," Phys. Rev. Lett. **99**, 017401 (2007).
32. V. M. Orera, J. I. Peña, A. Larrea, R. I. Merino, and P. B. Oliete, "Engineered self-organized microstructures using directional solidification of eutectics," Ceramics Trans. **225**, 185–196 (2011).
33. V. M. Orera and A. Larrea, "NaCl-assisted growth of micrometer-wide long single crystalline fluoride fibres," Opt. Mater. **27**, 1726–1729 (2005).
34. D. A. Pawlak, S. Turczynski, M. Gajc, K. Kolodziejak, R. Diduszko, K. Rozniatowski, J. Smalc, and I. Vendik, "How far are we from making metamaterials by self-organization," Adv. Funct. Mater. **20**, 1116–1124 (2010).

#161382 - $15.00 USD Received 12 Jan 2012; revised 19 Apr 2012; accepted 23 Apr 2012; published 15 Jun 2012
(C) 2012 OSA

35. J. Llorca and V. M. Orera, "Directionally solidified eutectic ceramic oxides," Prog. Mater. Sci. **51**, 711–809 (2006).
36. V. M. Orera, J. I. Peña, P. B. Oliete, R. I. Merino, and A. Larrea, "Growth of eutectic ceramic structures by directional solidification methods," J. Cryst. Growth (2011), doi:10.1016/j.jcrysgro.2011.11.056.
37. E. D. Palik, *Handbook of Optical Constants of Solids* (Academic Press Inc., 1985).
38. V. M. Orera, A. Larrea, R. I. Merino, M. A. Rebolledo, J. A. Valles, R. Gotor, and J. I. Peña, "Novel photonic materials made from ionic eutectic compounds," Acta Phys. Slovaca **55**, 261–269 (2005).
39. A. Larrea and V. M. Orera, "Porous crystal structures obtained from directionally solidified eutectic precursors," J. Cryst. Growth **300**, 387–393 (2007).
40. A. Larrea, L. Contreras, R. I. Merino, J. Llorca, and V. M. Orera, "Microstructure and physical properties of CaF2-MgO eutectics produced by the Bridgman method," J. Mat. Res. **15**, 1314–1319 (2000).
41. S. Foteinopoulou, M. Kafesaki, E. N. Economou, and C. M. Soukoulis, "Two-dimensional polaritonic photonic crystals as terahertz uniaxial metamaterials," Phys. Rev. B **84**, 035128 (2011).
42. J. C. Maxwell Garnett, "Colours in metal glasses and metal films," Phil. Trans. R. Soc. London Ser. A **203**, 385–420 (1904).
43. A. Sihvola, *Metamaterials Handbook. Theory and Phenomena of Metamaterials*, F. Capolino, ed. (CRC Press, 2009), Chap. 9.
44. A. Kirchner, K. Busch, and C. M. Soukoulis, "Transport properties of random arrays of dielectric cylinders," Phys. Rev. B **57**, 277–288 (1998).
45. J. A. Straton, *Electromagnetic Theory* (Wiley, 2007).
46. W. T. Doyle, "Optical properties of a suspension of metal spheres," Phys. Rev. B **39**, 9852–9858 (1989).
47. R. Ruppin, "Evaluation of extended Maxwell-Garnett theories," Opt. Commun. **182**, 273–279 (2000).
48. P. A. Belov, R. Marqués, S. I. Maslovski, I. S. Nefedov, M. Silveirinha, C. R. Simovski, and S. A. Tretyakov, "Strong spatial dispersion in wire media in the very large wavelength limit," Phys. Rev. B **67**, 113103 (2003).
49. K. C. Huang, P. Bienstman, J. D. Joannopoulos, K. A. Nelson, and S. Fan, "Phonon-polariton excitations in photonic crystals," Phys. Rev. B **68**, 075209 (2003).
50. K. C. Huang, P. Bienstman, J. D. Joannopoulos, K. A. Nelson, and S. Fan, "Field expulsion and reconfiguration in polaritonic photonic crystals," Phys. Rev. Lett. **90**, 196402 (2003).

1. Introduction

With the recent emerging technology of THz sources, such as Quantum Cascade Lasers (QCL) [1], the possibility of exploring and exploiting the THz regime of the electromagnetic spectrum becomes more and more appealing. This exploitation is of extreme technological interest as it can lead to a large variety of potential applications, ranging from tissue imaging [2], security and sensing [3], communications [4], and even astronomy [5].

The availability of THz radiation sources together with its immense technological potential applications highlight the need for THz manipulation components, as polarizers, filters, beam splitters, collimators, lenses, etc., which can not be achieved using the approaches employed in the optical regime, due to the non-strong-response of optical materials in the THz domain.

One possibility to overcome this situation is to employ metamaterials operating in the THz regime. Due to the variety of extraordinary electromagnetic properties that metamaterials can possess (like negative refractive index, backwards propagation, [6] etc.), and the associated possibilities that they offer (like, e.g. perfect in principle lensing [7]), along with the possibility to engineer their electromagnetic properties, can constitute a great tool for the manipulation of THz waves.

As it is well known, the main functional component of most of todays metamaterials is metal, and most of the fascinating metamaterial properties and possibilities are based on the negative permittivity response of the metal, resulting from the resonant free electron currents [8–10]. Besides that, it has been proposed that specific metamaterial properties, like artificial magnetism (leading to negative permeability) and negative refractive index, can be achieved also using high-index dielectrics instead of metals [11–13], where the role of the required current is undertaken by the strong displacement current.

A category of materials that can combine both the advantages of the metals and the high index dielectrics, and moreover, operate in the THz regime, are the so-called polaritonic materials

#161382 - $15.00 USD Received 12 Jan 2012; revised 19 Apr 2012; accepted 23 Apr 2012; published 15 Jun 2012
(C) 2012 OSA

[14]. Polaritonic materials are polar crystals where an incident electromagnetic wave can excite lattice vibrations (optical phonons) in the crystal. The coupling of the electromagnetic radiation with the transverse optical phonons, which occurs in the THz regime, can be described by a resonant electrical permittivity response of Lorenz type, characterized by both strong positive and negative permittivity regimes. This can make polaritonic materials a perfect replacement of either metals or high index dielectrics in the THz regime. Structuring thus properly such materials, one can achieve metamaterial properties like negative effective permeability [13, 15] or negative refractive index [12], and/or manipulate the dispersion of THz waves in unique ways, exploiting the interplay between material and structure (geometry) resonances.

Among the peculiar metamaterial properties that can be obtained with polaritonic materials, as we show in this work, is a hyperbolic dispersion relation [16–22]. A great possibility offered by hyperbolic dispersion relation structures is the possibility to achieve subwavelength resolution imaging [21–24], and even imaging with magnification [22]. This is based on the fact that hyperbolic dispersion relation does not have an upper limit in the value of the propagating wave-numbers that it can support; thus waves that are evanescent in free space (such waves carry the finest details of a source object) can couple to propagating waves in the hyperbolic dispersion structures and transfered without loss to the image plane. Moreover, shaping properly the dispersion relation in such structures one can lead to negative refraction for the propagating modes, achieving thus both evanescent and propagating modes convergence at the image plane.

The typical example of hyperbolic dispersion relation systems is uniaxial anisotropic systems where one of the permittivity (or one of the permeability) components is negative and the others positive. Such a uniaxial system (known as indefinite medium) can be realized, under certain conditions, using a two-dimensional periodic system of metallic nanowires or a layered (lamellar) metal-dielectric system (see, e.g. Ref. [25] and refs. there in). Indeed, up to now, metamaterials with hyperbolic dispersion relation [16–22] have been demonstrated in the optical regime using metallic nanorod arrays [26] or properly shaped metal-dielectric layers, leading also to imaging with magnification [21, 22]. Here we will demonstrate such dispersion in the THz regime using systems of polaritonic rods in a host.

A large obstacle in the current research and applications of metamaterials in THz, is the difficulty in the fabrication of the required structures, which should be of length scale from micrometers to nanometers. The most common todays fabrication approaches are lithographic approaches, which are time consuming, expensive, and are mainly restricted to planar geometries [27–30]. One promising way to go beyond the restrictions of the lithographic approaches for the creation of THz and optical metamaterials, is to employ self-organization approaches [31–34]. Self-organization approaches are usually simple, inexpensive and can be used for an easy and large scale production. Such a self-organization approach which can be proved extremely suitable for achieving polaritonic metamaterial structures is, as shown in this work, the directional solidification of eutectic mixtures [32–34]. Using this approach one can easily obtain self-organized systems of 1D, 2D or 3D symmetry, and of a large variety of geometrical patterns of the basic building blocks. Directionally solidified eutectics are composites with fine and homogeneous microstructures fabricated from melt. The microstructure and hence some of the material properties can be controlled by the solidification parameters and it is usually of fibrillar or lamellar morphology [35, 36]. The dimension of the single crystalline phases ranges from hundreds of micrometers to tens of nanometers depending on the growth rate. The volume filing fraction is fixed at the eutectic composition so phase size and interphase spacing are bound magnitudes in eutectics. Alignment along the solidification direction of the constituent crystalline phases induces anisotropic properties in otherwise isotropic composites. Depending of the materials composing the eutectic mixture (which can include any type of

#161382 - $15.00 USD Received 12 Jan 2012; revised 19 Apr 2012; accepted 23 Apr 2012; published 15 Jun 2012
(C) 2012 OSA

material, e.g. metals, magnetic materials, semiconductors etc.), the eutectics directional solidification approach can be used for creation of metamaterial microstructures of a rich variety of shapes and configurations [34], giving many possibilities in the metamaterials fabrication research.

In this paper we demonstrate the potential of the eutectics self-organization approach to give two-dimensional (2D) periodic systems of polaritonic rods embedded in a polaritonic host material, of varying system length scale (rod diameter from tens of microns to sub-micron). Moreover, determining the electromagnetic properties of the systems obtained, both with simulations and measurements, we show that part of those systems are characterized by a hyperbolic dispersion relation, which makes them suitable for THz superlensing and sensing applications. The particular polaritonic systems that we demonstrate here are alkali-halide systems made of LiF rods in KCl host and LiF rods in NaCl host [33].

The paper is organized as follows: In Section 2, we discuss the preparation (fabrication) of the eutectic samples along with the main properties of the component materials. In Section 3 we present the experimental, computational and theoretical characterization approaches that we use to analyze the electromagnetic wave propagation in those samples. In Section 4 we present and discuss the experimental and computational reflection studies of the samples that have been obtained, and we compare them with results obtained from an effective medium description of the samples. Finally, in Section 5 we discuss the hyperbolic dispersion response of the samples and in Section 6 we present our conclusions.

2. Eutectic metamaterial samples obtained

As was mentioned in the introduction, two different sets of eutectic metamaterial samples were fabricated and studied: Samples of LiF rods in KCl host, where the LiF volume filling fraction is 6.95%, and samples of LiF rods in NaCl, with LiF filling fraction of 25%.

All three polaritonic materials involved in these samples, i.e. LiF, NaCl and KCl, possess phonon-polariton resonances (photon induced excitations of transverse phononic modes within the crystal) in the THz region of the electromagnetic spectrum. In Fig. 1 we have plotted both the real and imaginary parts of the dielectric response function for these three materials at the frequency regime of the phonon-polariton resonance. The open circles in Fig. 1 represent the experimental data taken from Palik [37], while the continuous lines represent a fit (using least squares method) of the data, using a Lorentzian formula given by

$$\varepsilon(\omega) = \varepsilon_\infty - \frac{(\varepsilon_0 - \varepsilon_\infty)\,\omega_T^2}{\omega^2 - \omega_T^2 + i\,\omega\gamma}\,. \tag{1}$$

In Eq. (1), ω_T is the phonon-polariton resonance frequency, and ε_∞ and ε_0 are the limiting values of the dielectric function at frequencies much larger than $(\varepsilon_0 - \varepsilon_\infty)^{1/2}\omega_T$, and at zero frequency, respectively. The fitting parameters obtained from the fitting procedure for the three materials are shown in Table 1.

In Fig. 1 we see that LiF possesses a phonon-polariton resonance close to 9 THz (bottom graph), while for KCl (middle graph) and NaCl (top graph) the phonon-polariton resonances are at neighboring frequencies: 4.2 THz for KCl and 4.9 THz for NaCl.

2.1. Sample preparation

The eutectic samples were prepared by the directional solidification technique, using the Bridgman method [33]: 99.98% pure LiF (*Alfa Aesar*), 99.5% pure KCl (*Merk*) and 99.99% pure NaCl (*Alfa Aesar*) were used as starting powders. They were mixed in their eutectic composition: 91 wt% of KCl and 9 wt% of LiF for the LiF rods in KCl (samples named below as LK#), and 71 wt% NaCl and 29 wt% LiF for the LiF in NaCl (samples named LN#). The numbers

#161382 - $15.00 USD Received 12 Jan 2012; revised 19 Apr 2012; accepted 23 Apr 2012; published 15 Jun 2012
(C) 2012 OSA

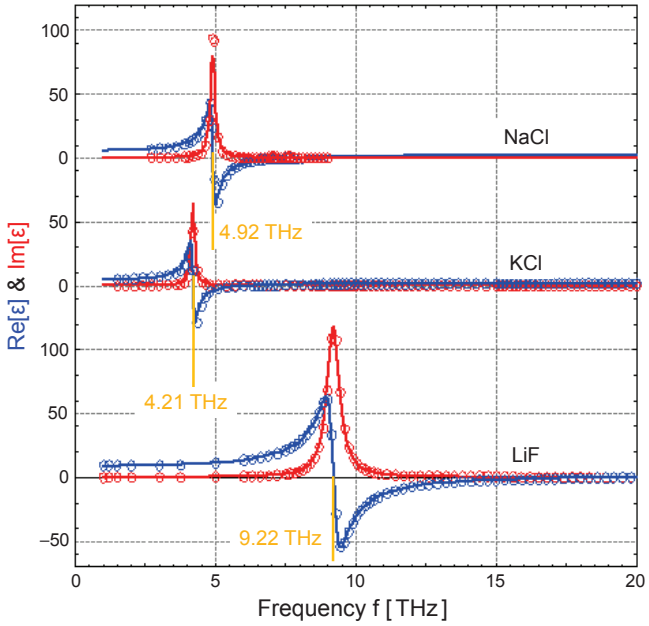

Fig. 1. Real (blue) and imaginary (red) parts of the dielectric response function for LiF, KCl and NaCl polaritonic materials. The open circles represent experimental measured data obtained from Palik [37], and the continuous lines result from the fitting of those data using Eq. (1) and the parameters in Table 1.

Table 1. Fitting parameters of dielectric function for LiF, NaCl and KCl, using a Lorentzian formula.

	Polaritonic materials		
Fitting parameters	**LiF**	**NaCl**	**KCl**
ε_0	8.705	5.586	4.430
ε_∞	2.027	2.222	2.045
$f_T = \omega_T/2\pi$ [THz]	9.22	4.92	4.21
$\gamma' = \gamma/2\pi$ [THz]	0.527	0.207	0.156

in the sample acronym indicate the interphase spacing. The growth was done in carbon-glass crucibles under an Ar atmosphere, pulling them out from the hot region of the furnace through a thermal gradient of 40 C/cm, at different pulling rates. Modifying the pulling rate has as a result the modification of size and inter-spacing of the LiF rods formed. Larger pulling rates result to smaller length-scale systems. The volume percent of fibers (LiF) remains fixed by the eutectic composition (6.9% for LiF in KCl and 25% for LiF in NaCl).

Transverse and longitudinal slices of the prepared samples were cut from the ingots, and polished with abrasive grain size of 1 μm or 0.25 μm, for microstructural characterization. Under the naked eye the slices looked as in Fig. 2(a). They appear rather transparent to transmitted light along the solidification direction, as corresponds to well aligned microstructures. Figures 2(c) (transmission optical micrograph) and 2(d) (scanning electron microscopy (SEM) image) show images of typical transverse cross sections of both eutectics, where the dark phase is LiF

#161382 - $15.00 USD Received 12 Jan 2012; revised 19 Apr 2012; accepted 23 Apr 2012; published 15 Jun 2012
(C) 2012 OSA

and the bright one is NaCl [Fig. 2(c)] and KCl [Fig. 2(d)]. As expected, the microstructure (see Fig. 2) consists of LiF rods embedded in a KCl or NaCl matrix. In Fig. 2(b) we show a SEM image, where one can appreciate the continuity of the LiF rods coming out of a humidity corroded longitudinal section of KCl-LiF. In fact, LiF fibers as long as several millimeters result [33,38], corresponding to large eutectic grains. Figures 2(c) and 2(d) indicate a nearly hexagonal arrangement of the LiF rods (short range order), forming though a rather polycrystalline system.

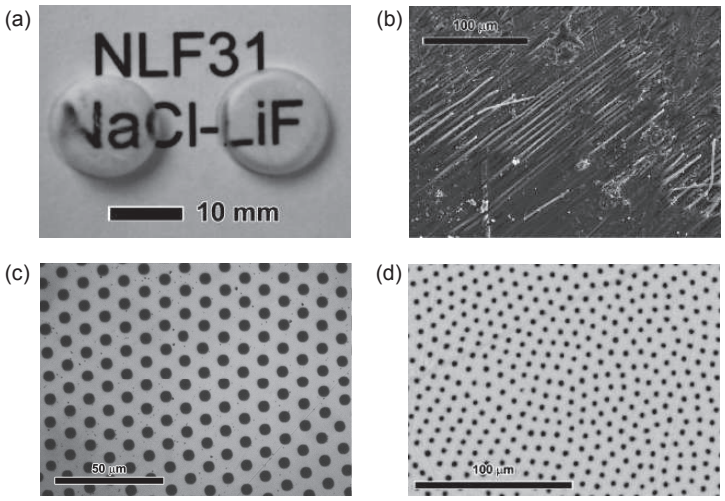

Fig. 2. (a) Slices of the eutectic NaCl-LiF cut transverse to the ingot and polished. The high transparency is the result of a good alignment of the fibers along the solidification direction; (b) SEM micrograph of longitudinal cut of KCl-LiF sample, partially corroded by ambient water vapor; (c) transverse cross-section of sample LN10.5 (NaCl-LiF eutectic, transmission optical micrograph); (d) transverse cross-section of sample LK7.8 (KCl-LiF eutectic, SEM micrograph).

There are several technological issues that may result in different scale of long-range ordering, rod separation and alignment across one sample (ingot). The best long range ordering is obtained when perturbations of the growth front are minimum, that is, intermediate growth rates for a particular growth equipment and method, that prevents constitutional undercooling or excessive macroscopic curvature of the growth front (that might arise at large growth rate or at the shortest spacing [39]); or temperature or mechanical instabilities (that might arise at the slowest growth rate or largest interphase spacing, for example in sample LK23.3, see below).

Statistics of interphase spacing (distance between the centers of the LiF rods) and rod diameters have been obtained by measuring them on different SEM micrographs, through a full transverse cross-section sample (i.e. sample cut perpendicular to the rod axes). Specifically, the LiF rod center to center distances were determined from fast Fourier transform (FFT) of the grey scale SEM images of transverse cross section of samples. In Fig. 3(a) we show a characteristic diameter distribution of our samples, showing a single peak in a quite narrow distribution, indication of the good sample quality. The only deviation from this result is encountered in samples of interphase spacing larger than 20 μm (grown at slower pulling rates). Such a case is shown in Fig. 3(b), concerning a LiF-KCl sample of interphase spacing 23.3 μm, where the diameter distribution shows clearly two peaks, indicating two different populations of diameters.

Samples with different interphase spacing (lattice constant of the hexagonal arrangement),

#161382 - $15.00 USD Received 12 Jan 2012; revised 19 Apr 2012; accepted 23 Apr 2012; published 15 Jun 2012
(C) 2012 OSA

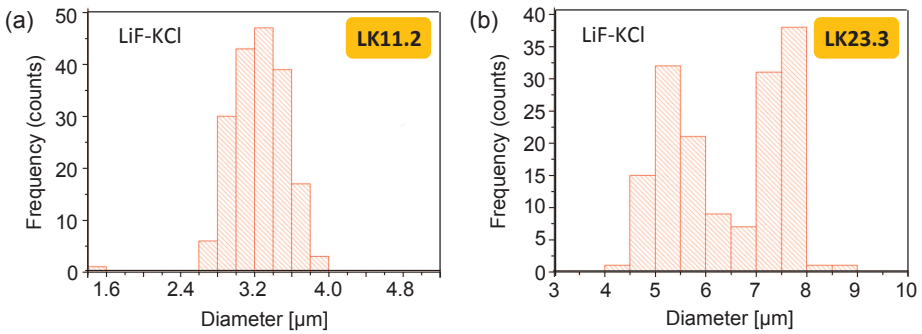

Fig. 3. Diameter distributions in KCl-LiF samples of interphase spacing (a) 11.2 μm and (b) 23.3 μm.

ranging from around 3 to 23 μm, were chosen for optical characterization. The geometrical features of the samples chosen are listed in Table 2 for the KCl-LiF samples and in Table 3 for NaCl-LiF ones. The errors indicate standard deviation of the corresponding magnitude. In the case of KCl-LiF systems, the volume filling fraction of LiF was 6.95% and the diameters were within the range 0.8 μm - 6.4 μm, while the separation distances between cylinders were within the range 2.8 μm – 23.3 μm (see Table 2). For the NaCl-LiF systems the volume filling fraction of LiF was 25%, with diameters of the cylinders between 2.0 μm – 10.7 μm and separation distances 3.6 μm – 20.3 μm (see Table 3). Standard deviation of the evaluated microstructural magnitudes are larger in LiF-KCl than in LiF-NaCl. This is particularly evident for the interphase spacing as obtained from FFT images. Also, the almost hexagonal ordering tends to extend a bit further in distance in LiF-NaCl than in LiF-KCl. This is consistent with qualitative observations in other fibrous directionality solidified eutectics, suggesting that small volume of the dispersed phase (as in LiF-KCl or MgO-CaF_2 [40]) results always in poorer long range ordering of the microstructure.

Table 2. Cylinder diameter and interphase distances (average distance between nearest neighbors rod centers) in the KCl-LiF samples. Errors are standard deviations of the image analysis.

LiF rods embedded in KCl host		
Sample acronym	**Interphase spacing [μm]**	**Rod diameter [μm]**
LK23.3	23.3 ± 3.9	6.4 ± 1.1
LK11.2	11.2 ± 2.3	3.2 ± 0.3
LK8.1	8.1 ± 1.1	2.6 ± 0.2
LK7.8	7.8 ± 1.2	2.1 ± 0.1
LK2.8	2.8 ± 0.4	0.8

When the samples are grown at a sufficiently slow pulling rate (leading to large rod diameters [33]), the cylindrical LiF fibers actually do not exhibit exactly a circular cross section, rather a hexagonal-like one. However, for simplicity, in our simulations we treat the rods as circular cylinders, knowing that the influence of the hexagonal geometry in the cross-section of the cylinders will be a slightly blue-shift in the cylinder resonances.

#161382 - $15.00 USD Received 12 Jan 2012; revised 19 Apr 2012; accepted 23 Apr 2012; published 15 Jun 2012
(C) 2012 OSA

Table 3. Cylinder diameter and interphase distances (average distance between nearest neighbors rod centers) in the NaCl-LiF samples. Errors are standard deviations of the image analysis.

LiF rods embedded in NaCl host		
Sample acronym	**Interphase spacing [μm]**	**Rod diameter [μm]**
LN20.3	20.3 ± 0.7	10.7
LN10.5	10.5 ± 0.3	5.5
LN6.1	6.1 ± 0.2	3.3 ± 0.2
LN3.6	3.6 ± 0.3	2.0 ± 0.1

3. Experimental setup and both theoretical and numerical tools employed

3.1. Experimental setup used to measure reflectance

The experimental electromagnetic characterization of our samples was performed using specular reflectance measurements at nearly normal incidence. The specular reflectance was measured in the range of 3.3 THz to 11 THz, using a commercial *Bruker IFS 66v/S FT-IR* spectrometer. Longitudinal slices (i.e. cuts parallel to the rods) of thickness around 1 mm were cut and dry-polished for optical measurements. Typically the surface of the slices was 10×10 mm^2. Only the sample LN3.6 had smaller area (around 4×10 mm^2), since the well aligned region for this fast-pulled out sample had a smaller size. The reflectance for both parallel polarization (incident electric field, $\mathbf{E}_{inc}$, parallel to the rod axes) and perpendicular polarization ($\mathbf{E}_{inc}$ perpendicular to the rod axes) was measured, as indicated in Fig. 4(a) and 4(b) respectively, with the wave vector of the incident radiation, $\mathbf{k}_{inc}$, being always perpendicular to the axes of the rods, i.e. in the plane of periodicity. The reflectance measurements were performed at incidence angle $\theta_{inc} = 13°$ in respect to the vector normal to the interface (see Fig. 4), which is the smallest achievable angle of incidence of the instrument.

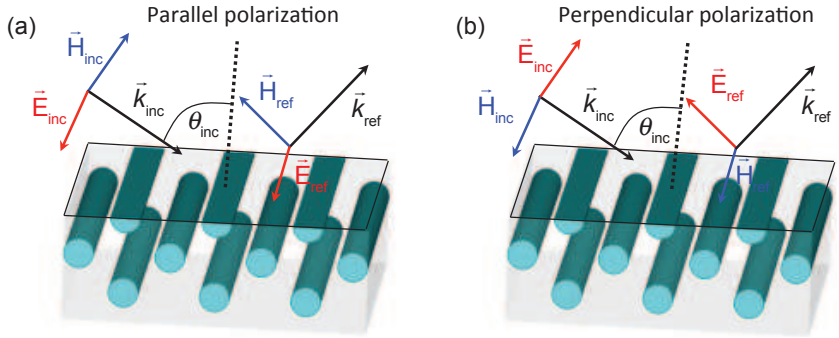

Fig. 4. Schematics of (a) parallel and (b) perpendicular polarization configurations measured.

3.2. Models used for numerical calculations of the reflectance

The numerical characterization of the samples was done mainly through calculations of transmission and reflection from finite thickness systems. We modeled each eutectic system as a set of infinitely long parallel circular cylinders in 2D hexagonal arrangement, as shown in Fig. 5.

#161382 - $15.00 USD Received 12 Jan 2012; revised 19 Apr 2012; accepted 23 Apr 2012; published 15 Jun 2012
(C) 2012 OSA

We considered propagation in the plane of periodicity (i.e. in the plane perpendicular to the cylinder axes) and we calculated the transmission and reflection under normal incidence, for both parallel and perpendicular polarization [see Fig. 5(a)]. The calculations were performed using the commercial software *CST Microwave Studio*, which solves numerically Maxwell equations in both time- and frequency-domain, employing the Finite Integration Technique based on the space and time discretization of Maxwell's equations in their integral form.

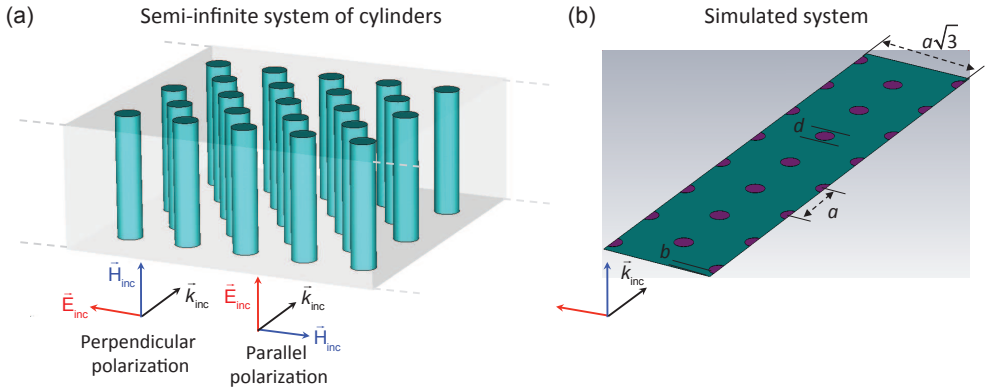

Fig. 5. (a) Sketch of the model for the eutectic metamaterial system used in numerical calculations. The cylinders were considered as LiF circular rods with hexagonal arrangement, embedded either in KCl or NaCl host. (b) A transverse cut of the computational cell employed in most of the calculations presented here. The cell consists of 7 unit cells along propagation direction, while periodic boundary conditions along the other directions have been considered. *a* is the unit cell size (lattice constant) and *d* is the rod diameter.

The dielectric functions used to characterize rods and hosts during the calculations were the fitted Lorentzian expressions given by Eq. (1), with fitting parameters those of Table 1.

For each polarization and sample studied, we performed simulations modifying the length of the computational cell along propagation direction, to guarantee convergence of the results assuring that they represent correctly the behavior of an optically thick system. The results presented here have been obtained for a system of seven unit cells along propagation direction (ΓK direction of the hexagonal lattice), as shown in Fig. 5(b), while periodic boundary conditions along the other directions have been employed.

3.3. Analytical model: effective medium approach

The idea beneath an effective medium approach is to remove the highly oscillating electromagnetic fields inside a system by a suitable averaging procedure, and thus replacing the inhomogeneous system by a homogeneous one characterized by effective response functions. Such an approach is extremely useful in the electromagnetic characterization of metamaterials, as it can give a simple way to characterize and understand the behavior and the possibilities of each particular system.

The validity though of such approach is guaranteed only in the limit of low filling fraction of the scattering units comprising the system or in the long wavelength limit compared to the inter-spacing of these scattering units, where strong multiple scattering and diffraction of the waves is quite restricted. The precise frequency regime where these conditions are fulfilled for any particular system is not easy to be identified and it is highly dependent on the system itself (component materials, filling fractions, etc.).

#161382 - $15.00 USD Received 12 Jan 2012; revised 19 Apr 2012; accepted 23 Apr 2012; published 15 Jun 2012
(C) 2012 OSA

A useful approach to identify the applicability of effective medium descriptions for uniaxial anisotropic systems, as the ones discussed here, has been proposed recently in Ref. [41], where a couple of conditions, related with the insensitivity of the effective material parameters from the system thickness and propagation direction, have been provided. An important result of Ref. [41] for uniaxial anisotropic systems is that once these conditions are fullfilled for polarization purely perpendicular and for polarization purely parallel, then the validity of homogeneous effective medium description for arbitrary polarization and propagation direction is ensured.

In this work, we test the validity of homogeneous effective medium description for our samples when the propagation is in the plane of periodicity, for both perpendicular and parallel polarization. The effective medium description that we employ when the electric field (**E**) is perpendicular to the cylinders axes is the well known Maxwell Garnett model, suitable for dispersed particles inside a matrix [42, 43]. The Maxwell Garnett formula for the effective dielectric response function in two dimensions is given by

$$\varepsilon_{eff}^{\perp}(\omega) = \varepsilon_{host}(\omega)\frac{(1+\varphi)\,\varepsilon_{cyl}(\omega)+(1-\varphi)\,\varepsilon_{host}(\omega)}{(1-\varphi)\,\varepsilon_{cyl}(\omega)+(1+\varphi)\,\varepsilon_{host}(\omega)}, \tag{2}$$

where φ is the volume filling fraction of the cylinders, and ε_{host} and ε_{cyl} are the permittivities of the host and the cylinders, respectively. When **E** is parallel to the cylinder axes, the appropriate formula for the effective dielectric function is the average dielectric function [44], given by

$$\varepsilon_{eff}^{||}(\omega) = \varphi\,\varepsilon_{cyl}(\omega)+(1-\varphi)\,\varepsilon_{host}(\omega). \tag{3}$$

The way to test the validity of the above response functions in our systems is to examine if these functions can reproduce the reflection characteristics obtained from the experiment and the simulations. Once ensured the applicability of these particular effective medium models in our systems, we can further use these models to predict propagation and dispersion characteristics which are of particular merit for metamaterial applications.

4. Electromagnetic characterization results and discussion

Using the approaches described in the previous section, we measured and calculated the reflectance from the two different sets of eutectic metamaterials obtained: LiF rods embedded in a KCl matrix, with LiF filling fraction of 6.95% (five different samples), and LiF rods embedded in a NaCl matrix (four different samples), with LiF filling fraction of 25%.

4.1. Reflectance from KCl-LiF eutectic metamaterial systems

In Fig. 6 we present the reflection results obtained for the LiF rods in KCl samples LK11.2, LK8.1, LK7.8 and LK2.8 (see details of each sample in Table 2). We report the analysis of sample LK23.3 separately, since this sample differs from the others in the sense that its diameter distribution show clearly two peaks [see Fig. 3(b)].

In Fig. 6 we have split the results into two columns. The left column corresponds to parallel polarization in respect to the axes of cylinders, while the right column to perpendicular polarization. On top of each column we show a plot of the effective electrical permittivity as a function of frequency, both real (blue) and imaginary (red) parts, corresponding to each polarization case (obtained from Eq. (2) for the right column and Eq. (3) for the left column). We have indicated with an orange-shaded region the frequency region where the real part of the effective dielectric permittivity is negative for each polarization, which is the frequency range where one expects to have large reflectivity from the samples.

For parallel polarization (left column), we see two separate regions where $\mathrm{Re}[\varepsilon] < 0$: around 5 THz and around 10 THz. The lower-frequency region corresponds to the reflectance due to

#161382 - $15.00 USD Received 12 Jan 2012; revised 19 Apr 2012; accepted 23 Apr 2012; published 15 Jun 2012
(C) 2012 OSA

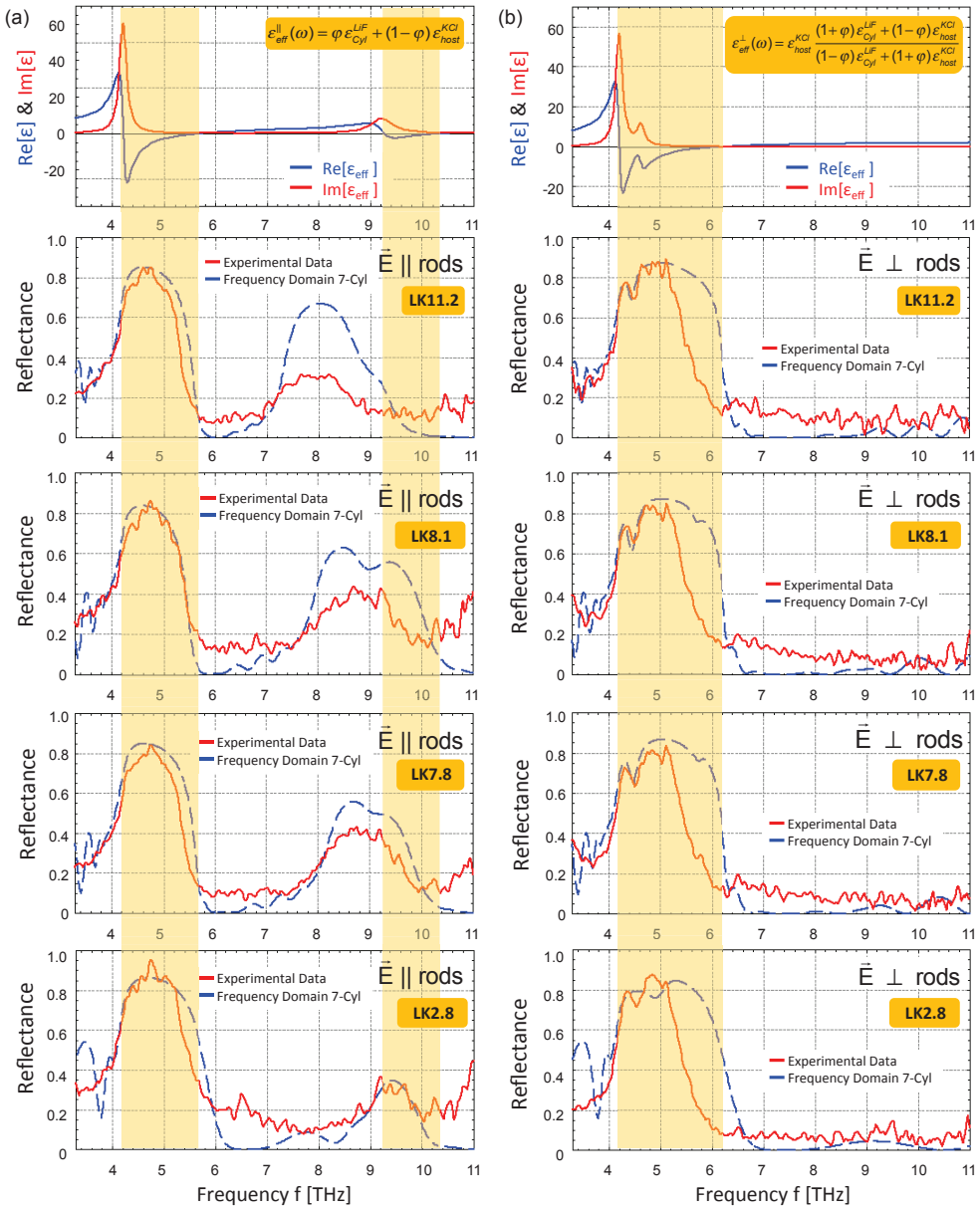

Fig. 6. Comparison between experimentally-measured reflectance and both simulation results and effective medium predictions for the KCl-LiF systems. Left column (a) shows results for parallel polarization and right column (b) for perpendicular polarization in respect to the axes of cylinders in the sample. First row shows the real and imaginary parts of the effective electrical permittivity for each polarization, and orange-shaded regions highlight the frequency regimes where the real part of the permittivity is negative.

#161382 - $15.00 USD Received 12 Jan 2012; revised 19 Apr 2012; accepted 23 Apr 2012; published 15 Jun 2012
(C) 2012 OSA

the KCl matrix, while the higher-frequency region is due to the contribution of the LiF rods. For the perpendicular polarization (right column), we observe that Maxwell Garnett formula predicts $\mathrm{Re}[\varepsilon] < 0$ in a single broader frequency region, from 4.2 THz up to 6.2 THz, with a peak at around 4.5 THz, where $\mathrm{Re}[\varepsilon]$ is less negative and the losses are smaller than those for smaller frequencies.

In Fig. 6, below the effective permittivity plots, we show both the measured and simulated reflectance for each sample, as a function of frequency. We have superimposed to the experimental reflectance plot (shown in red and measured at an incidence angle of 13°), in each case and for both polarizations, the results from the simulations (shown in dash-blue and obtained at normal incidence).

As a general trend, we see that for all samples in parallel-polarization configuration (left column) there is a very good agreement between the positions of the measured reflectance peaks with the simulated ones. Moreover, there is a good agreement in the low-frequency high-reflectance regime (centered around 5 THz) between the prediction of the effective medium formula and both the experimental and simulation results. However, this simple effective medium model predicts accurately the position of the second reflectance peak, coming from the cylinders, only in the case of the smaller lattice constant sample, LK2.8. For samples with larger lattice constant, the prediction of the effective medium model becomes less and less accurate, as the second reflectance peak appears at lower frequencies. This inaccuracy does not signify though failure of the samples to be described as homogeneous effective media but rather the failure of the particular effective medium approach employed. The reason is that this particular model (average permittivity and Maxwell Garnett approach) has been obtained in the limit where $k_{host}R$, $k_{cyl}R$ and $k_{eff}R$ are all much smaller than unity (k denotes the wavenumber in each material and R the cylinder radius). In this limit the main contribution to the cylinder scattering in the parallel polarization case is the isotropic scattering term (of zero angular momentum) and no cylinder resonance exists in frequencies below the LiF polaritonic-resonance frequency ($f_T = 9.22$ THz).

Indeed this is the case for scatterers of radius smaller than 0.5 μm, as shown in Fig. 7(a), where we show the single-cylinder extinction cross-section [45] for a LiF cylinder of radius 0.4, 1.05, 1.6 and 3.3 μm, (for **E** parallel to cylinder axis). As can be seen from Fig. 7(a), as we go to cylinders of larger radii, the lowest-frequency resonance (coming from the isotropic scattering), which for very small radius is located at f_T, moves to frequencies below f_T and additional resonances start to appear in the close-by regime. This is due to the large values of the LiF permittivity below f_T, which make the quantity $k_{cyl}R\,(=(\omega/c)\sqrt{\varepsilon_{cyl}}R = 2\pi R/\lambda_{cyl})$ comparable to unity (leading to resonances in this frequency regime) even for quite small cylinder radius, bringing thus the system beyond the regime of validity of the average effective permittivity and the Maxwell Garnett approach.

In such cases of high index rods in lower index host, and in the limit where $k_{host}R$, $k_{eff}R << 1$ but $k_{cyl}R \approx 1$, a correct homogenization approach should take into account the full single-cylinder scattering (not only the first/isotropic term) and not the limit $k_{cyl}R \to 0$. Such an approach, known as extended Maxwell Garnett approach [46, 47], has been applied already in the case of spherical polaritonic scatterers [15], and has predicted even magnetic activity (leading to negative permeability) in those systems in the frequency regimes of high dielectric constant of the spheres. An analogous approach, based on proper field-averaging [11], has been applied in the case of SiC rods in a host and has predicted not only magnetic activity but simultaneously negative permittivity and permeability, leading to negative index of refraction, a behavior demonstrated also experimentally [12]. Negative permeability and negative refractive index behavior though requires rods of quite high permittivity and large filling fraction. In our systems neither the LiF permittivity just below the polaritonic resonance is high enough nor the LiF

#161382 - $15.00 USD Received 12 Jan 2012; revised 19 Apr 2012; accepted 23 Apr 2012; published 15 Jun 2012
(C) 2012 OSA

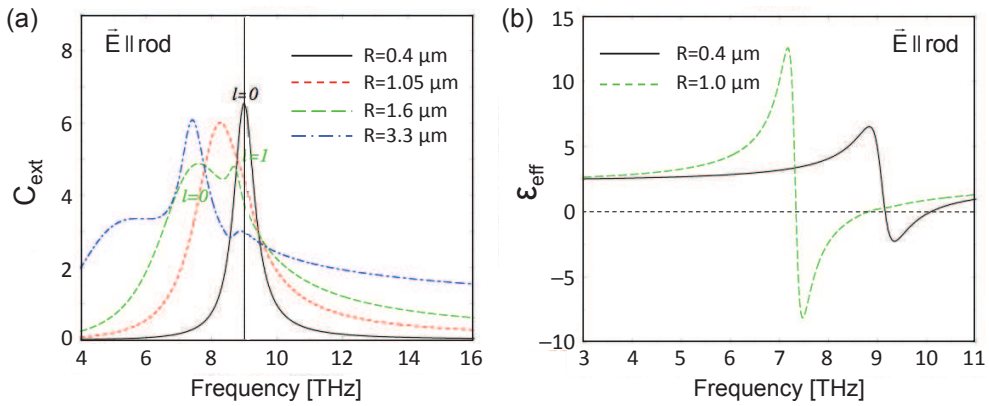

Fig. 7. (a) Single LiF cylinder extinction cross-section (normalized with the cylinder diameter) in a host with $\varepsilon = 2$ for parallel polarization. Legends show the radius of the cylinder. The numbers l close to some extinction peaks denote the order of the cylindrical harmonic modes which are responsible for those peaks. (b) Effective permittivity calculated using the approach of Ref. [11] for a system of LiF cylinders of radius R in a host with $\varepsilon = 2$, with LiF volume fraction 6.95%.

filling fraction is sufficient to obtain negative permeability, as is confirmed applying the field-averaging approach of Ref. [11] in our systems. What is confirmed though [see Fig. 7(b)] is the shift of the negative effective permittivity regime originated from the rods to lower frequencies as the rod radius is increased. For rods of radius 1.6 μm, as in our LK11.2 system, the negative permittivity regime predicted by the averaging approach lies between 7 and 9 THz, coinciding with the second reflection peak of the sample LK11.2 (see Fig. 6), and showing that even in that system an homogeneous effective medium approximation can be applied.

The above mentioned approaches, although can nicely describe the behavior of our composites, they are not associated through simple analytical formulas allowing an easy parametric investigation and interpretation of the behavior of the systems. This is the reason why we focus here mostly on Maxwell Garnett and average permittivity formulas.

For sample LK2.8, as was already mentioned, the Maxwell Garnett and average permittivity models predict satisfactorily the position and intensity of the reflection spectrum, for both polarizations. This is demonstrated in more detail in Fig. 8, where we have superimposed the experimental reflection data and the reflection predicted from the effective medium models.

Returning to Fig. 6, another observation is that for parallel polarization (left column) the relative intensity of the second reflectance band (coming from the LiF-rods) versus the intensity of the KCl-matrix band is smaller in the experimental than in the simulation results. The difference increases as the rod diameter (or interphase spacing) increases. This is in agreement with the fact that the second band is a result of a resonance, thus it is expected to fade away when the LiF rod diameter is no longer unique but distributes with a moderate standard deviation (see Tables 2 and 3).

In Fig. 6, in the reflectance data obtained from the simulations we also see quick oscillations, clearly seen in the lower frequency range from 3.3 THz to 4 THz for both polarizations, and also in the higher-frequency range, from 8 THz to 11 THz, for the perpendicular polarization (right column in Fig. 6). These oscillations increase in frequency as we increase the length of the computational cell in the propagation direction, and in this sense they are the result of interference phenomena from the internal reflections at both ends of the sample, that is, Fabry-Pérot

#161382 - $15.00 USD Received 12 Jan 2012; revised 19 Apr 2012; accepted 23 Apr 2012; published 15 Jun 2012
(C) 2012 OSA

resonances. This was confirmed by modifying slightly the total length of the computational cell and examining the change in the spectral position of those oscillations.

It can be also observed in Fig. 6 that the first lower-energy measured reflectance peaks are systematically narrower than both the simulated reflectance peaks and what is expected from the effective medium models; this is more evident for the perpendicular polarization (right column in Fig. 6). We believe that this effect is due to the fact that we are using a fit of the experimental data (Palik [37]) for the dielectric response function of the polaritonic materials, without considering the contribution of multiphonon transitions to the dielectric function (higher order modes). Although these higher-order modes are faint in the dielectric response function, they give rise to absorptions on the high-frequency region of the dispersion and a bit less negative real dielectric response function, both effects diminishing the reflectance intensity.

The above explanation is confirmed in Fig. 8, where the reflection obtained from the homogeneous "effective slab" has been calculated using both the Lorentz fitted data for the dielectric response function of the materials involved (see Table 1) and directly the experimental Palik [37] data. The simulated spectra using the data tabulated by Palik reproduce more accurately the measured reflectance for the KCl-LiF system, while the ones using the Lorenz fitted data lead to broader resonances.

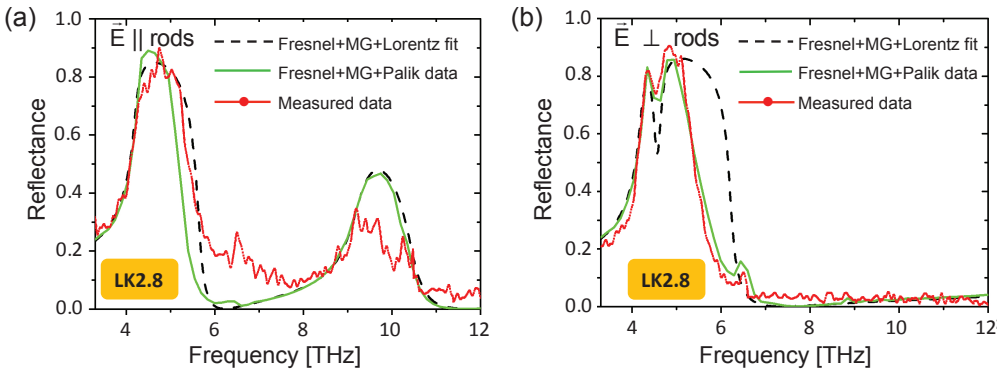

Fig. 8. Comparison between measured reflectance data for the system LK2.8, and the reflectance predicted by applying Fresnel formulas in a homogeneous "effective" slab of the same thickness, where the effective parameters have been calculated using both Lorentz-fitted data and Palik data for the permittivities of KCl and LiF. Reflectance for (a) parallel and (b) perpendicular polarization in respect to the axes of cylinders.

We present and discuss next, the results for sample LK23.3, where the agreement between experimental and theoretical results is poor, indicating the limitation of both our numerical characterization approach and the effective medium theories. Sample LK23.3 was grown at the slowest pulling rate, as discussed in Section 2, and present different features than the rest of the samples, by showing clearly a two-peaks diameter distribution [see Fig. 3(b)]. Even thought this sample can not be characterized by a single average diameter of the LiF fibbers, we attempt to perform numerical simulations of its reflectance by considering three different scenarios: We considered three different values of a single average diameter of the cylinders and average separation distances between them (while keeping fixed the volume filling fraction), assuming periodicity for each calculation for feasibility of the calculations. The simulations were performed for (i) d=5.4 μm [the average diameter of the left peak of the distribution shown in Fig. 3(b)], (ii) d=6.6 μm (the average value of the diameter for the entire distribution) and (iii) d=7.8 μm [the right peak in Fig. 3(b)]. The results are presented in Fig. 9, separated in

#161382 - $15.00 USD Received 12 Jan 2012; revised 19 Apr 2012; accepted 23 Apr 2012; published 15 Jun 2012
(C) 2012 OSA

two columns: left one for parallel polarization and right one for perpendicular polarization. As in Fig. 6, the first row corresponds to the real (red) and imaginary (blue) parts of the effective dielectric permittivity for each polarization case, using average and Maxwell Garnett formulas. We clearly see in Fig. 9 that the agreement between experiment and numerical results is poor, mainly for the parallel polarization (left column in Fig. 9), and that the reflection results deviate strongly from the predictions of the simple homogeneous effective medium models employed. In fact the presence in the simulations of many distinct, narrow and closely aligned reflectance peaks indicates (not confirms though) failure of any homogeneous effective medium approach, thus being clear that this specific sample does not possesses a hyperbolic dispersion relation.

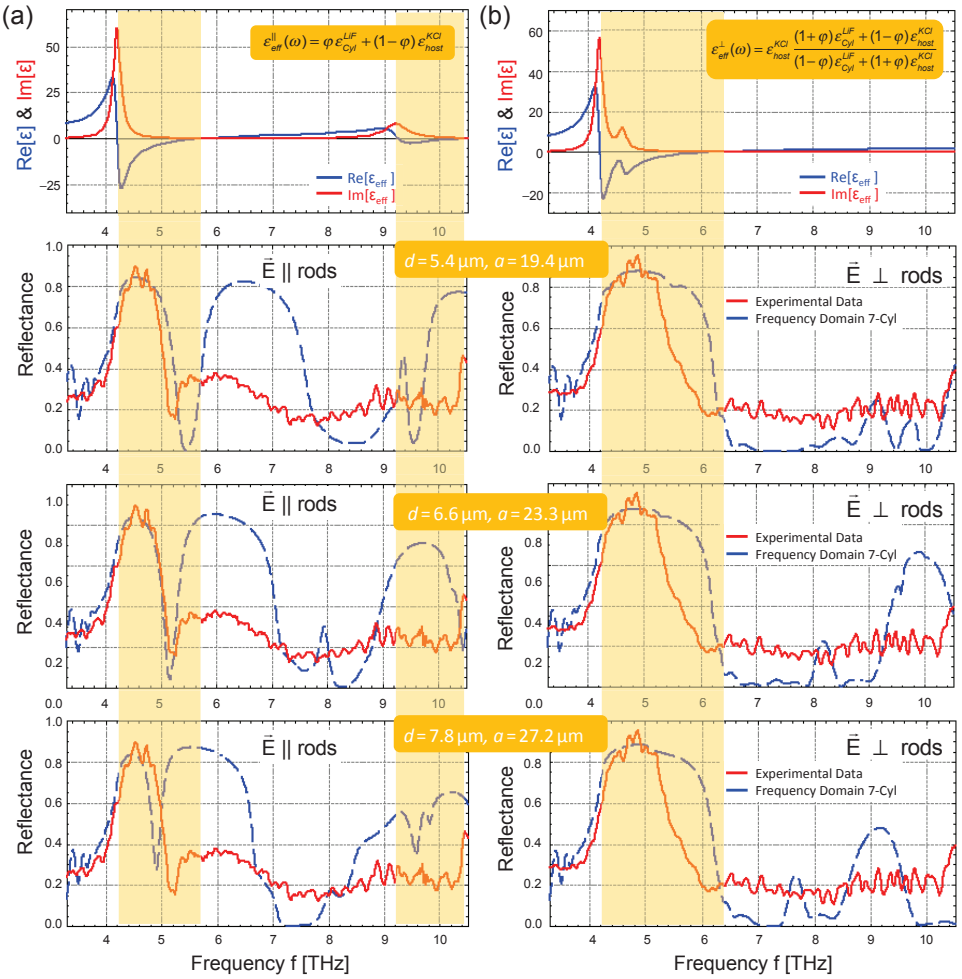

Fig. 9. Comparison between experimentally-measured reflectance and both simulation results and analytical models for sample LK23.3. Left column (a) shows results for parallel polarization and right column (b) for perpendicular polarization, in respect to the axes of cylinders in the sample. The simulated results concern the cylinder diameters (d) and lattice constants (a) shown in the legends. Filling fraction is always 6.95%. The top row shows the effective permittivity versus frequency and the orange-shaded regions highlight the regimes where that permittivity is negative.

#161382 - $15.00 USD Received 12 Jan 2012; revised 19 Apr 2012; accepted 23 Apr 2012; published 15 Jun 2012
(C) 2012 OSA

4.2. Reflectance from NaCl-LiF eutectic metamaterial systems

The main difference between the NaCl-LiF systems and the KCl-LiF systems discussed here, is in the volume filling fraction of the LiF rods; while in the NaCl-LiF case the LiF filling fraction is 25%, for KCl-LiF case it is close to 7%. This implies that, since the separation distances between neighboring cylinders are similar to the KCl-LiF case, the diameters of the cylinders are larger in the NaCl-LiF case (see Tables 2 and 3).

The study of the NaCl-LiF systems is summarized in Fig. 10, where we show together the experimental and simulated (using *Microwave Studio*) reflection data for four representative samples: LN20.3, LN10.5, LN6.1 and LN3.6.

In the first row of Fig. 10 we have also included the effective dielectric response function of the system, obtained through Eqs. (3) and (2), indicating with an orange-shaded region the frequency regimes where $\mathrm{Re}[\varepsilon] < 0$ for both parallel and perpendicular polarizations, in respect to the axes of the cylinders. For a direct comparison of the reflection results with the effective medium predictions, we have added in the last row of Fig. 10 the reflection from a thick "effective" homogeneous slab (green line), with the effective parameters obtained through Eqs. (3) and (2), using in this case the LiF and NaCl permittivities directly (without fit) from Palik data [37].

As a general trend, we see that both experimental and simulated reflectance show a more complicated spectral dependence than in the KCl-LiF system. For parallel polarization and for samples LN10.5, LN6.1 and LN3.6 (third, fourth and fifth rows in left column in Fig. 10), we have reasonable agreement between the experimental reflection peak coming from the matrix material (peak at around 5.2 THz) and the simulated data. For the smaller-scale samples we also see good agreement of the reflection with what is expected from the effective medium models.

For the larger-scale samples, the polydispersity in the rod diameters and in the orientation of the polycrystals in the samples, results in the elimination (smoothing out) of the narrow-band reflection characteristics in the experimental data, observed in the simulations.

As in the KCl-LiF system case, we also see here the Fabry-Pérot interference phenomenon superimposed in the simulated results for both polarizations. Another similarity between the two systems is that systematically the experimental peaks are narrower than the simulated ones. We believe that the explanation is what it was mentioned before for the KCl-LiF case, i.e. due to the fact that we are using a fit of the dielectric response function for both NaCl and LiF polaritonic materials, and this fit does not reproduce accurately the permittivity in the regimes where $\mathrm{Re}[\varepsilon] \approx 0$.

5. Polaritonic systems as indefinite media

In the previous section we have presented the reflectance spectra (experimental and simulated) from slabs of the eutectic systems KCl-LiF and NaCl-LiF. These alkali-halide eutectics present a hexagonal arrangement of aligned LiF rods (of 6.95% volume filling fraction in the KCl matrix and 25% in the NaCl matrix), with varying lattice parameter. We also showed that the effective medium model represented by Eqs. (2) and (3) (Maxwell Garnett and average permittivity model) predicts reasonably well, both in band position and relative intensity, the reflectance spectra for the samples with the smaller length-scale (like samples LK2.8 and LN3.6) for both polarizations in respect to the axes of the rods. Moreover, according to the theoretical results presented in Ref. [41], the effective parameters obtained through Eqs. (2) and (3) are independent of the angle of incidence and therefore they constitute a valid effective medium description of those samples. Thus these eutectic samples will be fully described by an effective permittiv-

#161382 - $15.00 USD Received 12 Jan 2012; revised 19 Apr 2012; accepted 23 Apr 2012; published 15 Jun 2012
(C) 2012 OSA

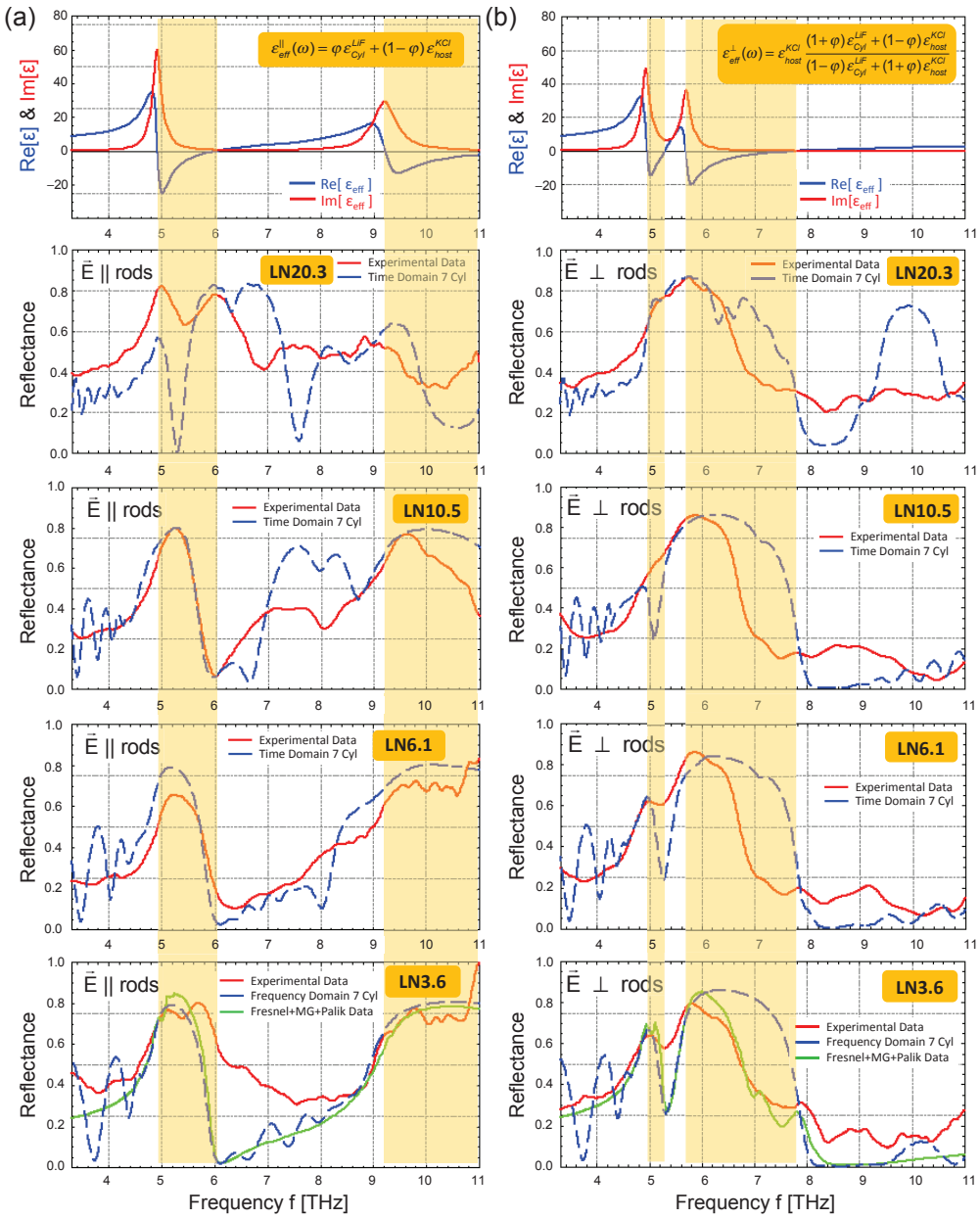

Fig. 10. Comparison between experimentally-measured reflectance and both simulation results and analytical models for the LiF rods in NaCl host systems. Left column (a) shows results for parallel polarization and right column (b) for perpendicular polarization, in respect to the axes of the rods in the sample. In both cases the propagation is in the plane of periodicity. First row shows the real and imaginary parts of the effective dielectric permittivity for each polarization. The orange-shaded regions highlight the negative effective permittivity regimes.

#161382 - $15.00 USD Received 12 Jan 2012; revised 19 Apr 2012; accepted 23 Apr 2012; published 15 Jun 2012
(C) 2012 OSA

ity tensor of the form

$$\begin{pmatrix} \varepsilon_{eff}^{\perp} & 0 & 0 \\ 0 & \varepsilon_{eff}^{\perp} & 0 \\ 0 & 0 & \varepsilon_{eff}^{||} \end{pmatrix} \tag{4}$$

and dispersion relations, $\omega(\mathbf{k})$,

$$\varepsilon_{eff}^{\perp}\frac{\omega^2}{c^2} = k_x^2 + k_y^2 + k_z^2, \qquad \frac{\omega^2}{c^2} = \frac{k_x^2 + k_y^2}{\varepsilon_{eff}^{||}} + \frac{k_z^2}{\varepsilon_{eff}^{\perp}} \tag{5}$$

for the ordinary (left equation) and the extraordinary (right equation) wave, respectively (considering the cylinder axes along $\hat{z}$-direction).

In Fig. 11 we replot the real part of the effective permittivity tensor components $\varepsilon_{eff}^{\perp}$ and $\varepsilon_{eff}^{||}$ (obtained from Eqs. (2) and (3)) as a function of frequency, for both systems: Fig. 11(a) for KCl-LiF and Fig. 11(b) for NaCl-LiF.

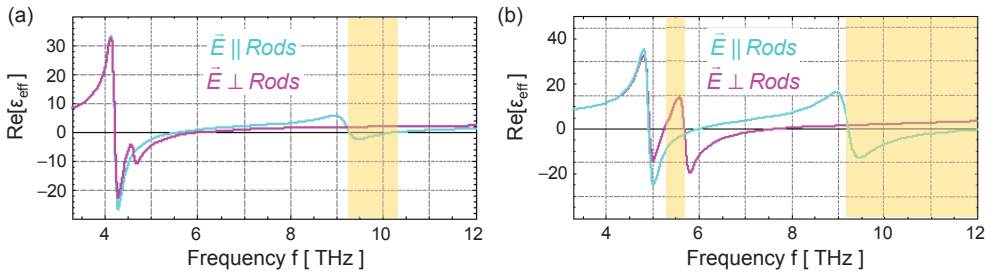

Fig. 11. Effective dielectric response function for (a) KCl-LiF system and (b) NaCl-LiF system, as a function of frequency, for both polarizations: parallel and perpendicular to the axes of the LiF cylinders.

For the KCl-LiF case [Fig. 11(a)], the orange-shaded region at around 10 THz denotes the range of frequencies where the dielectric function is negative for **E** parallel to the rods (metal-like behavior), while it is positive for **E** perpendicular to the rods (dielectric behavior). In this region thus, the sample will behave as an anisotropic uniaxial medium with a negative permittivity component (indefinite medium), and thus it will be characterized by a hyperbolic dispersion relation. Hyperbolic dispersion relation, as was discussed in the introduction, gives great possibilities for subwavelength imaging applications. Such a dispersion relation has been discussed and realized so far only in the case of metallodielectric systems, while it has been discussed only recently [41] and not realized at all in the case of polaritonic systems.

Polaritonic systems offer a natural and easy way to achieve hyperbolic dispersion relation in the THz and far-infrared part of the electromagnetic spectrum, avoiding the strong spatial-dispersion effects [48], that one has to face in analogous systems made of metallic components (spatial dispersion effects act detrimentally to the hyperbolic dispersion relation). Moreover, in polaritonic composites one can achieve, in the same system, frequency regimes of negative (effective) permittivity, of very high permittivity values and/or of regular permittivity, and both the permittivity values and the associated frequency regimes can be tuned by changing the rod size, giving thus unique possibilities for dispersion engineering. For example, for the case of Fig. 6, when the diameter of the cylinder is increased the negative permittivity regime which is at ~ 9.5 THz in sample LK2.8 is shifted downwards. The shift is as large as 1.5 THz going from the sample LK2.8 to the sample LK11.2 (diameter from 0.8 μm to 3.2 μm – see Table 2).

#161382 - $15.00 USD Received 12 Jan 2012; revised 19 Apr 2012; accepted 23 Apr 2012; published 15 Jun 2012
(C) 2012 OSA

In the NaCl-LiF system [Fig. 11(b)] the situation is even more rich: We see that there are two frequency regions satisfying the criteria $\mathrm{Re}[\varepsilon_{eff}^{||}] < 0$ and $\mathrm{Re}[\varepsilon_{eff}^{\perp}] > 0$ (a narrow one from 5.3 to 5.7 THz, and a broader one from 9.2 THz up to around 12 THz – both highlighted with orange-shaded region) and one region where $\mathrm{Re}[\varepsilon_{eff}^{\perp}] < 0$ and $\mathrm{Re}[\varepsilon_{eff}^{||}] > 0$ (5.8 – 7.5 THz), offering thus great possibilities to tune the hyperbolic dispersion both in shape and frequency. This way, besides highly controlled superlensing, one can achieve other peculiar optical phenomena [41, 49, 50] like low-loss propagation, strong field confinement or expulsion, angle dependent polarization, frequency dependent propagation direction allowing the realization of beam splitters, etc., combined with the possibility to study or achieve many different optical responses using the same system.

6. Conclusions

In this work, using eutectics directional solidification, we have fabricated polaritonic eutectic systems made of LiF rods periodically placed in KCl and NaCl hosts, with varying system lattice size. These eutectic systems have been characterized experimentally and investigated theoretically, and it was shown that most of them behave as indefinite media (anisotropic uniaxial media with a negative permittivity component) in the THz regime and that the spectral range where this effect appears can be tailored by more than 1.5 THz, by selecting the appropriate lattice parameter for the eutectic (growth conditions). This opens the field for the search of other eutectic systems that provide different spectral windows and phenomenology.

Acknowledgments

Authors would like to acknowledge fruitful discussions with Dr. Thomas Koschny, as well as the financial support by EU under the project NMP4-SL-2008-213669-ENSEMBLE. MFA also acknowledges financial support of the Ministerio de Educación (Spain) under the FPU scholarship program and ARC acknowledges financial support of Consejo Nacional de Ciencia y Tecnología (Mexico).

#161382 - $15.00 USD Received 12 Jan 2012; revised 19 Apr 2012; accepted 23 Apr 2012; published 15 Jun 2012
(C) 2012 OSA